Assessment of liver steatosis and fibrosis in rats using integrated coherent anti-Stokes Raman scattering and multiphoton imaging technique

Jian Lin
Fake Lu
Wei Zheng
Shuoyu Xu
Dean Tai
Hanry Yu
Zhiwei Huang

Assessment of liver steatosis and fibrosis in rats using integrated coherent anti-Stokes Raman scattering and multiphoton imaging technique

Jian Lin,ª Fake Lu,ª Wei Zheng,ª Shuoyu Xu,b Dean Tai,c Hanry Yu,c,d,e,f and Zhiwei Huangª
ªNational University of Singapore, Optical Bioimaging Laboratory, Department of Bioengineering,
Faculty of Engineering, Singapore 117576
bSingapore-MIT Alliance, Computational and System Biology Program, Singapore 117576
cInstitute of Bioengineering and Nanotechnology, Singapore 138669
dNational University Health System, Yong Loo Lin School of Medicine, Department of Physiology, Singapore 117597
eMechanobiology Institute, Singapore 117411
fMassachusetts Institute of Technology, Department of Biological Engineering, Cambridge, Massachusetts 02139

Abstract. We report the implementation of a unique integrated coherent anti-Stokes Raman scattering (CARS), second-harmonic generation (SHG), and two-photon excitation fluorescence (TPEF) microscopy imaging technique developed for label-free monitoring of the progression of liver steatosis and fibrosis generated in a bile duct ligation (BDL) rat model. Among the 21 adult rats used in this study, 18 rats were performed with BDL surgery and sacrificed each week from weeks 1 to 6 ($n = 3$ per week), respectively; whereas 3 rats as control were sacrificed at week 0. Colocalized imaging of the aggregated hepatic fats, collagen fibrils, and hepatocyte morphologies in liver tissue is realized by using the integrated CARS, SHG, and TPEF technique. The results show that there are significant accumulations of hepatic lipid droplets and collagen fibrils associated with severe hepatocyte necrosis in BDL rat liver as compared to a normal liver tissue. The volume of normal hepatocytes keeps decreasing and the fiber collagen content in BDL rat liver follows a growing trend until week 6; whereas the hepatic fat content reaches a maximum in week 4 and then appears to stop growing in week 6, indicating that liver steatosis and fibrosis induced in a BDL rat liver model may develop at different rates. This work demonstrates that the integrated CARS and multiphoton microscopy imaging technique has the potential to provide an effective means for early diagnosis and detection of liver steatosis and fibrosis without labeling. © *2011 Society of Photo-Optical Instrumentation Engineers (SPIE)*. [DOI: 10.1117/1.3655353]

Keywords: coherent anti-Stokes Raman scattering; second harmonic generation; two-photon excitation fluorescence; microscopy; steatosis; fibrosis; bile duct ligation; hepatic fat; collagen fibrils; liver.

Paper 11362R received Jul. 12, 2011; revised manuscript received Sep. 18, 2011; accepted for publication Sep. 29, 2011; published online Nov. 10, 2011.

1 Introduction

Fatty liver is a common disease representing the excessive triglyceride accumulation in hepatocytes.[1] Its pathogenesis includes factors, such as the abuse of alcohol, obesity, and resistance to insulin.[2] Among various types of liver disease, non-alcoholic fatty liver disease is the most prevalent disease that affects over 10% of the world population and more than half in obese people.[2] Further, fatty liver disease may develop from subtle steatosis into steatohepatitis, liver fibrosis, cirrhosis, and eventually hepatocellular carcinoma (HCC).[1] Liver fibrosis is another common liver ailment that arises from chronic insults to the liver with the accumulation of extracellular matrix proteins (mainly collagens), resulting in cirrhosis, portal hypertension, liver failure, and HCC.[3] Diagnosis of liver disease at an early stage is crucial to improving the survival rates of the patients at high risk. Quantitative characterizations of hepatic fatty cells and collagen fibrils in liver tissue are essential to improving early detection of liver fibrosis and steatosis as well as for effective clinical treatments. Tissue biopsy with histological

examinations currently remains the gold standard for assessment of liver diseases, but it is invasive and impractical for a mass screen of high-risk patients.[4] Moreover, this method depends on the staining efficiency, which may induce uncertainties in the diagnosis. Conventional biomedical imaging techniques, such as ultrasonography, computed tomography, and magnetic resonance imaging, have been widely used to detect liver disease, but mostly at advanced stages.[4] None of these imaging techniques provides sufficient sensitivity, spatial resolution, and specificity for detecting and staging liver disease at an early stage.

Recently, nonlinear optical microscopy imaging techniques, such as two-photon excitation fluorescence (TPEF), second-harmonic generation (SHG), and coherent anti-Stokes Raman scattering (CARS), which possess many attractive features such as three-dimensional (3D) sectioning capability at submicrometer scale resolutions, deep tissue penetration depth, and non-destructiveness with biochemical specificity, have emerged as a powerful tool for label-free imaging in cells and tissue.[5–10] TPEF signals arise from the intrinsic molecules in hepatocyte, such as fiber elastins, NAD(P)H, and FAD, emitting intense fluorescence under excitation. These molecules are related to the cell metabolism,[11] making TPEF microscopy suitable to image

Address all correspondence to: Zhiwei Huang, National University of Singapore, Faculty of Engineering, Optical Bioimaging Laboratory, Department of Bioengineering, 9 Engineering Drive 1, Singapore 117576 Singapore; Tel: +(65) 6516-8856; Fax: +(65) 6872-3069; E-mail: biehzw@nus.edu.sg.

tissue and cell morphologies.[5] SHG microscopy that is sensitive to the noncentrosymmetric microstructures has been utilized to probe collagen fibrils in tissue.[9,10] CARS microscopy that permits selective imaging of specific biomolecular vibrations has proven to be particularly useful for imaging lipid-rich structures in biological and biomedical systems.[5–8] Due to the differences in contrast mechanisms and biochemical/biomolecular origins involved in each nonlinear imaging modality, the rapid acquisition of multimodal nonlinear microscopy imaging with spatial colocalization on the same tissue will provide new insights into various tissue constituents/structures for better tissue diagnosis and characterization. In this study, we report on the implementation of a unique integrated CARS and SHG/TPEF microscopy imaging technique developed to monitor the changes of biochemical and biomolecular constituents and structures (e.g., hepatic fats, collagen fibrils, and hepatocyte morphology) of liver tissue associated with the progression of liver steatosis and fibrosis induced in a bile duct ligation (BDL) rat liver model.

2 Methods

2.1 Animal Model and Tissue Preparations

Wistar rats were used in this study with an initial weight of 200 g. Animals were housed in the Animal Holding Unit of the National University of Singapore (NUS) with free access to laboratory chow and drinking water in a 12-h light, 12-h dark schedule. The study protocol was approved by the Institutional Animal Care and Use Committee at NUS. To induce liver fibrosis and steatosis, the BDL of rats was performed under general anesthesia with ketamine and xylazine.[12,13] A midline abdominal incision was performed to explore the liver and intestines. The bile duct was then ligated near the portal veins with silk. The wound was then closed with a double layered tissue closure with vicryl sutures. A total of 18 rats were ligated and sacrificed each week from weeks 1 to 6 ($n = 3$ per week). Three control rats were also sacrificed at week 0. The fresh liver tissues harvested were immediately frozen in liquid nitrogen, and sectioned into a series of 10 to 20-μm tissue slides in a microtome cryostat (HM 500 OM, Carl Zeiss, Germany) for multimodal nonlinear microscopy imaging. The conventional histopathology on the sectioned liver tissue slides for grading liver fibrosis and steatosis were also conducted. To evaluate the penetration depth of backward (epi-) CARS imaging, week 6 liver tissues were also excised (~2 mm in thickness) in this study.

2.2 Histopathological Method

The 10-μm thick liver tissue slices were stained with a Masson Trichrome (MT) stain kit (ChromaView advanced testing, 87019, Richard-Allan Scientific, Thermo Fisher Scientific, Wathan, Massachusetts) for histopathological examination. Liver fibrosis scoring was determined using a modified Ruwart score system.[14,15] Fat-specific stainings on sectioned liver tissues for liver steatosis examination were also performed using standard Oil Red O staining (ORO, Sigma-Aldrich Pte Ltd., Singapore).
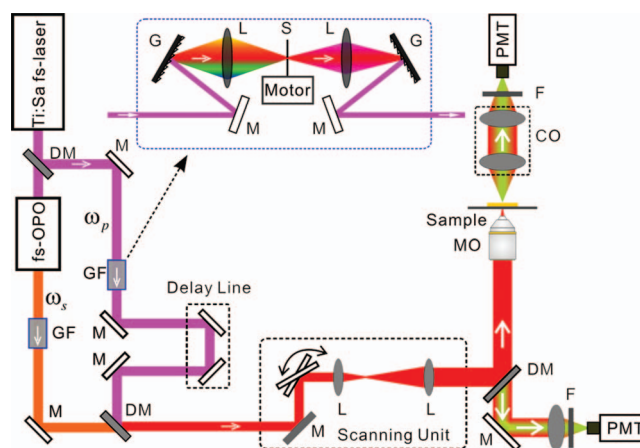

Fig. 1 Schematic diagram of the integrated fs/ps swappable CARS and multiphoton (SHG/TPEF) microscopy developed for label-free tissue imaging. The switching between fs/ps laser pulse trains can be readily realized by using the 4-f paired grating spectral filtering module. For ps-CARS, the wavelengths of pump and Stokes beams are 835 and 1095 nm, respectively; whereas the average powers of pump and Stokes beams are 6 and 3 mW, respectively. For fs-TPEF and SHG, the excitation wavelength is tuned to 835 nm with an average power of ~10 mW. DM, dichroic mirror; L, lens; M, mirror; GF, paired gratings-based filtering module; MO, microscope objective; CO, Condenser; F, filter set [700-nm short-pass and 670-nm band-pass (FWHM 10 nm) filters for CARS; 450 to 700-nm bandpass filter for TPEF; 415-nm band-pass (FWHM 10 nm) filter for SHG]; PMT, photomultiplier tube; G, grating; S, slit.

2.3 Multimodal Nonlinear Optical Microscopy

Figure 1 shows the schematic of the integrated multimodal nonlinear optical microscopy (including CARS, SHG, and TPEF imaging) platform developed for label-free tissue imaging. A 100-femtosecond (fs) Ti:sapphire laser (Mira 900, Coherent Inc.) is used as the pump source for SHG and TPEF imaging.[5] For CARS imaging, the fs laser beam is divided into two parts by a beam splitter: one beam works as the pump beam; the other beam is used to pump an optical parametric oscillator (OPO) (Coherent Inc.) to produce the Stokes beam for CARS microscopy. A dual 4-f paired-grating spectral filtering (inset in Fig. 1) was employed to enable readily conversion of the 100-fs laser pulse trains into transform-limited 1-picosecond (ps) pulses in the spectral range of 700 to 1600 nm.[7] The spectrally shaped pump and Stokes beams are collinearly combined through a dichroic mirror (SWP-45-RU1080-TU830, CVI), and delivered into a confocal laser scanning microscope (FV300, Olympus) with a customized nondescan epi-detection channel, and then focused onto the sample by a microscope objective (UPlanSApo 40×, N.A. 0.9, Olympus) for high contrast ps-CARS imaging. On the other hand, high quality tissue SHG and TPEF images can also be acquired in tandem under the same imaging platform by simply swapping the 4-f grating filtering from the ps mode to the fs mode. For the forward detection, the nonlinear optical signal radiation from the sample is collected by a condenser (U-TLD, NA 0.9, Olympus) and detected by a photomultiplier tube (PMT) (R3896, Hamamatsu); for the epi-detection, the signals are collected by the same objective used for excitation (UPlanSApo 40×, NA 0.9, Olympus) and detected by another PMT (R3896, Hamamatsu). The maximum field of view (FOV) in this study is 350 × 350 μm, which

is determined by the focusing objective (40×) used; but by using lower magnification objectives, a larger FOV can also be achieved (e.g., 700 × 700 μm when using a 20× microscope objective). The throughput of our multimodal imaging system was calibrated using Rhodamine B in methanol solution (10^{-4} M) for TPEF imaging and a cover slip for CARS imaging.[16,17] One notes that the TPEF signal does not interfere with SHG imaging, as the 450- to 700-nm bandpass filter is used for TPEF, while the 415-nm bandpass filter (FWHM 10 nm) for SHG blocks the emission of major fluorophores in liver tissue [e.g., NADH and FAD (emission peaks are around 465 and 540 nm, respectively)].[11]

2.4 Image Acquisition and Data Processing

The single-plane and 3D images of all three nonlinear microscopy imaging modalities (i.e., CARS/SHG/TPEF) were acquired from 20-μm sectioned liver tissue slides for visualization and quantitative analysis. Single-plane images were acquired at 10-μm below the tissue surface, whereas the 3D images were acquired from the tissue surface down to 20 μm with 0.5 μm intervals. The field of view of the image was 300 × 300 μm. Five different sites for each sectioned tissue were imaged and averaged for intensity analysis. Each image (512 × 512 pixels, 2.71 s/image) was averaged for 5 times for achieving better signal to noise. During the image acquisition, the powers of pump and Stokes laser beams and the PMT gain were kept unchanged for each individual imaging modality. In ps-CARS imaging, background removal was done by subtracting the nonresonant images (taken at Raman shift of 2945 cm^{-1}) from the resonant images (taken at 2845 cm^{-1}).[7] For fs-SHG imaging, the background was removed by subtracting a prerecorded background image. The fs-TPEF images were not post-processed. To quantify the imaging results, the projection was first calculated by adding up all the images in a single 3D scanning; then the intensities of all pixels in the projection image were summed up to get the overall intensity value. One notes that the CARS intensities can be used to estimate the hepatic fat content (n_{fat}) by using the equation $n_{fat} \propto \sqrt{I_R - I_{NR}}$, where I_R and I_{NR} denote the resonant (Raman shift at 2845 cm^{-1} for CH$_2$ vibration) and nonresonant (2945 cm^{-1}) CARS intensities, respectively,[8] while SHG intensity can be used to evaluate the collagen content in tissue,[10] and TPEF intensity can be used to estimate the volume occupied by healthy hepatocytes related to cell metabolism.[11]

3 Results and Discussion

Figure 2 shows the comparisons between the histopathologically stained tissue images [Figs. 2(a) and 2(c)] and the corresponding CARS/SHG/TPEF images [Figs. 2(b) and 2(d)] of 10-μm sectioned tissues from week 6 BDL liver tissue samples. The TPEF image [Fig. 2(a)] of the sectioned liver tissue with lipid-specific ORO staining agrees very well with the CARS image [Fig. 2(b)] of the same tissue sites without staining, confirming that CARS imaging can directly probe hepatic lipid droplet distributions in liver steatosis tissue without labeling. Similarly, the collagen fiber distributions shown in blue color in the MT-stained liver tissue have also correlated well with the SHG signals of the same tissue sites [green color in Fig. 2(d)], affirming the utility of the
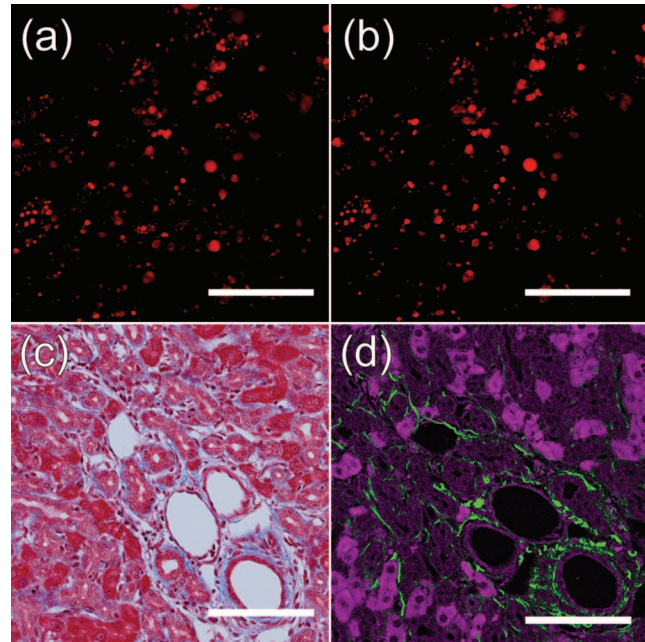

Fig. 2 Comparisons between stained tissue images and the corresponding CARS/SHG/TPEF images of 10-μm sectioned liver tissues of a week-6 BDL tissue sample. (a) Fat-specific ORO-stained TPEF image; (b) CARS image of the same tissue site without staining; (c) image obtained from a conventional MT stained liver tissue (blue color represents connective tissue such as collagen in liver; dark red and red colors show nuclei cytoplasm), and (d) merged SHG/TPEF image of the same liver tissue site (SHG: green color; TPEF: magenta color). Note that all images are taken in the forward direction. The scale bar in each image is 100 μm.

SHG technique for label-free imaging of collagen fibers in liver fibrosis tissue. Note that TPEF signals of liver tissue [magenta color in Fig. 2(d)] reveal the hepatocyte morphologies which coincide with the MT-stained tissue image [dark red and red colors in Fig. 2(c)]. Hence, multimodal nonlinear optical microscopy (i.e., CARS/SHG/TPEF) imaging can effectively identify specific biochemical compositions and cell morphologies of liver tissue without labeling.

Figure 3 shows the comparison of multimodal images of the control (normal) sectioned liver tissue (images in the first row of the panel from tissue in week 0) and pathologic liver tissues (images in rows 2 to 7 of the panel acquired from sectioned liver tissues in weeks 1 to 6, respectively, after BDL surgery). There are no significant hepatic lipids and collagen fibrils accumulations in normal liver tissue, as confirmed by CARS [Fig. 3(a1), symmetric CH$_2$ stretch vibration of hepatic lipids at 2845 cm^{-1}] and SHG [Fig. 3(a2)] images; and the hepatocyte morphologies remain regular distributions as identified by TPEF [mainly arising from NAD(P)H and flavins' autofluorescence[7]] in normal liver tissue [Fig. 3(a3)]. However, after the BDL surgery, the accumulations of hepatic lipid droplets and aggregated fibrillar collagen are clearly identified in CARS [Figs. 3(b1)–3(g1)] and SHG images [Figs. 3(b2)–3(g2)]; the hepatocyte morphologies become severely irregular (probably due to the bile ducts proliferation associated with severe hepatocyte necrosis[10]) as shown by the TPEF images [Figs. 3(b3)–3(g3)]. It is also observed that a large quantity of hepatic lipid droplets and collagen start to appear in the BDL liver tissue from week 3 onwards
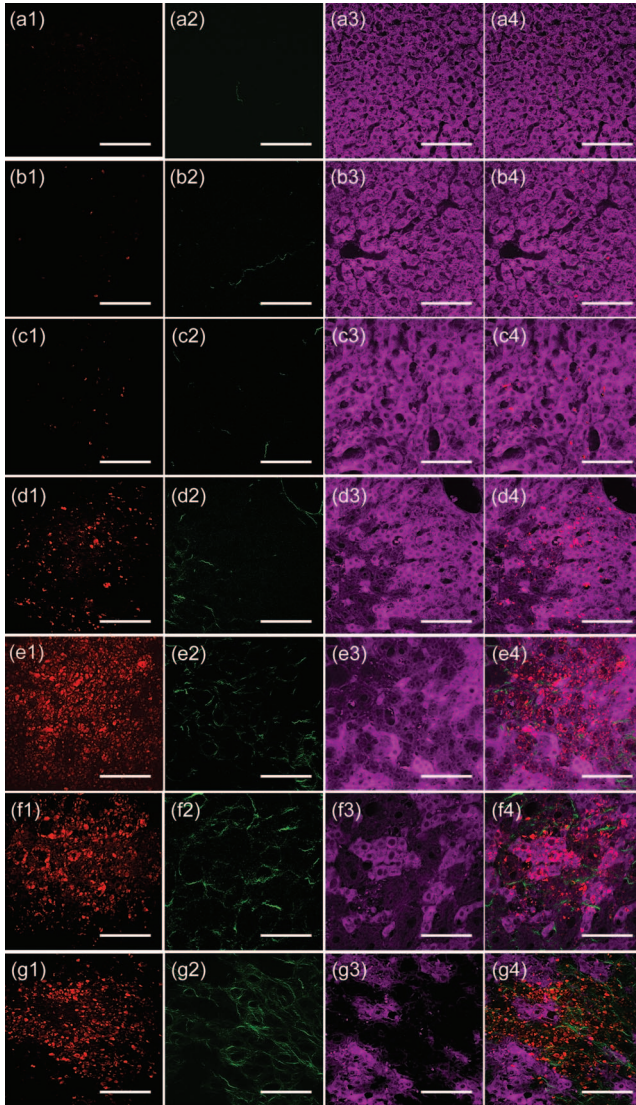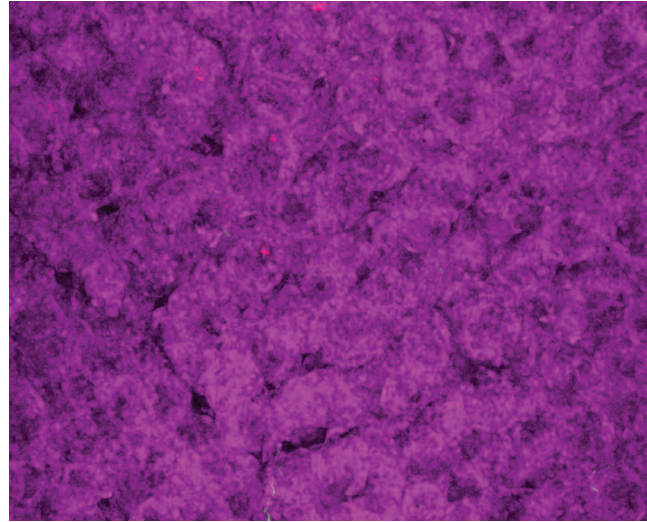
Fig. 3 Comparison of multimodal images of the control (normal) sectioned liver tissue (images in the first row of the panel from tissue in week 0) and pathologic liver tissues (images in rows 2 to 7 of the panel are acquired from sectioned liver tissues in week 1 to 6, respectively, after BDL surgery): Images [(a1)–(g1)] in the first column represent ps-based CARS images of lipid droplets (red); images [(a2)–(g2)] in the second column are fs-based SHG images of collagen fibrils (green) in liver tissue; images [(a3)–(g3)] in the third column stand for fs-based TPEF images of hepatocytes (magenta), and images [(a4)–(g4)] in the fourth column are the overlay of multimodal images (CARS/SHG/TPEF) of sectioned liver tissues. Note that the scale bar is 100 μm; and images were taken at 10-μm depth of the sectioned tissues.
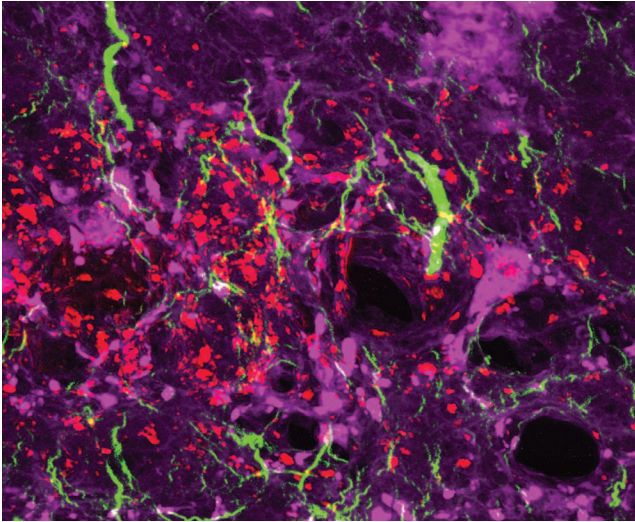
[Figs. 3(d1)–3(g1), 3(d2)–3(g2)]. The merged images (CARS, SHG, and TPEF) of normal and BDL liver tissues [Figs. 3(a4)–3(g4)] confirm that both liver steatosis and fibrosis can be effectively induced by the bile duct ligation surgery in the rat liver model. The collagen fibers are more preferentially generated in the regions where the hepatocyte morphologies are destroyed, which are also confirmed by histopathology image [Fig. 2(c)]; whereas the distribution of hepatic lipid droplets does not show the similar trend in fibrotic liver tissue. The above results suggest that the integrated CARS and multiphoton imaging can be

Video 1 Representative three-dimensional colocalized (CARS/SHG/TPEF) images of normal liver tissue, revealing the hepatic lipid droplets (red color in CARS image), aggregated collagen fibrils (green color in SHG), and hepatocyte morphologies (magenta color in TPEF) in the control rat liver model (week 0). The overall thickness of the 3D sectioned image of liver tissue is about 20 μm with a scanning interval of 0.2 μm. Image size: 250 × 200 × 20 μm. (MPEG, 7.4 MB). [URL: http://dx.doi.org/10.1117/1.3655353.1]

used to directly assess the progression of liver tissue changes associated with liver disease (e.g., fibrosis, steatosis) transformation.

Further, the 3D biochemical distributions in liver tissues can also be readily observed by imaging into different tissue depths using the integrated CARS/SHG/TPEF imaging technique. Video 1 shows an example of 3D intensity distributions of CARS, SHG, and TPEF signals in a 20-μm sectioned normal (control) rat liver tissue recorded in the forward direction. The normal hepatocytes visualized by TPEF signals are uniformly distributed throughout the normal tissue; whereas almost no CARS and SHG signals can be found, indicating no formation of hepatic lipid droplets and collagen fibrils in normal liver tissue. As a comparison, Video 2 shows an example of 3D distributions of hepatic lipid droplets (red color in CARS images), collagen fibrils (green color in SHG images), and cell morphologies (magenta color in TPEF images) in a 20-μm sectioned liver tissue in week 6 after BDL surgery. We can observe that TPEF signal intensities are much lower than that in the control tissue. The dark areas with weak TPEF intensities show the degenerated hepatocytes due to the lack of fluorescent molecules; and the bile duct proliferation is also revealed by the big black holes in the images (Video 2). CARS and SHG signals show that the aggregated collagen fibrils are highly cross-linked each other, forming the 3D networks ranging from 5 to 20 μm in thickness in BDL liver tissue, while the lipid droplets tend to randomly distribute across the collagen networks in BDL liver tissue within 10-μm thickness. The pathological development of liver steatosis and fibrosis, including hepatic lipid droplets, collagen fibers, bile duct, and hepatocyte morphologies, can be clearly visualized using the integrated CARS and multiphoton microscopy. Thus, the multimodal nonlinear microscopy imaging technique provides a novel label-free approach for sensitively probing

Video 2 Representative three-dimensional colocalized (CARS/SHG/TPEF) images of pathologic liver tissues, revealing the hepatic lipid droplets (red color in CARS image), aggregated collagen fibrils (green color in SHG), and hepatocyte morphologies (magenta color in TPEF) in the BDL rat liver model (week 6). The overall thickness of the 3D sectioned image of liver tissue is ~20 μm with a scanning interval of 0.2 μm. Image size: 250 × 200 × 20 μm. (MPEG, 11.3 MB). [URL: http://dx.doi.org/10.1117/1.3655353.2]

different biochemical changes of tissue in 3D with high spatial resolution.

To quantify the formation of hepatic fat and collagen fibrils as well as the hepatocyte necrosis induced by BDL in rat liver tissue, we calculated CARS, SHG, and TPEF intensities from the forward-detected CARS/SHG/TPEF images acquired at each week after BDL surgery. Figure 4(a) shows the changes of the contents of hepatic lipid droplets (the square root of CARS intensity), collagen fibrils (SHG intensity), and TPEF intensity in a BDL rat liver tissue at different time after BDL. The content of collagen fibers in a BDL rat liver tissue increases to over 4 folds at week 1 with respect to week 0, and keeps increasing up to ~20-fold higher in week 6; while the TPEF intensity keeps decreasing to half of that in week 0. These changes indicate that liver fibrosis occurs immediately after BDL operation and becomes more severe with the elapse of time; whereas the volume of normal hepatocytes keeps decreasing from weeks 1 to 6 (down to the value only half of that of the control liver tissues due to the hepatocyte degeneration and bile duct proliferation). But the lipid concentration increases to a maximum in week 4 (~30-fold higher in week 4 as compared to week 0), and then appears to stop growing and slightly decrease from weeks 4 to 6. The findings suggest that liver steatosis and fibrosis induced in the BDL rat liver model may develop in different rates. We have also evaluated the correlation of SHG intensities with conventional histopathological scores of liver fibrosis [Fig. 4(b)]. A highly linear relationship [dashed fit line in Fig. 4(b): $I_{SHG} = 0.84 I_{score} - 1.16$; correlation coefficient $R^2 = 0.99$] between SHG intensity versus histopathology scoring is observed. The similar linear relationship between CARS intensities versus Oil Red O staining intensities has also been found [Figs. 2(a) and 2(b)]. These findings reconfirm that SHG and CARS imaging can be employed to effectively estimate the collagen and lipid contents in liver tissue without staining, yielding the similar results as conventional histopathological methods.

To extend multimodal nonlinear optical microscopy imaging into possible *in vivo* biomedical applications, one of the imaging concerns is how deep and how much the nonlinear optical signals can be detected in the epi-direction. TPEF emission is nondirectional and can be easily collected in the epi-direction. Generally, most CARS and SHG signals from cells and tissue are
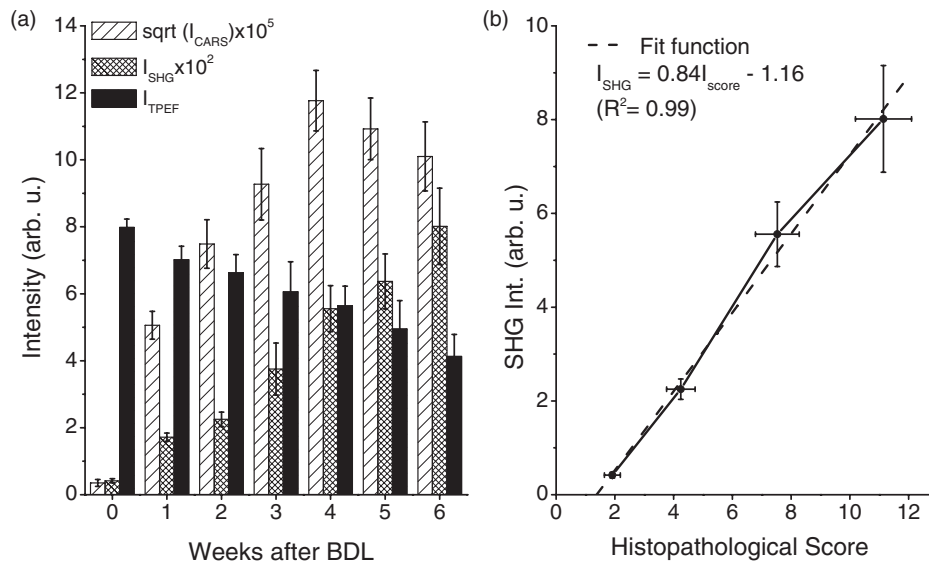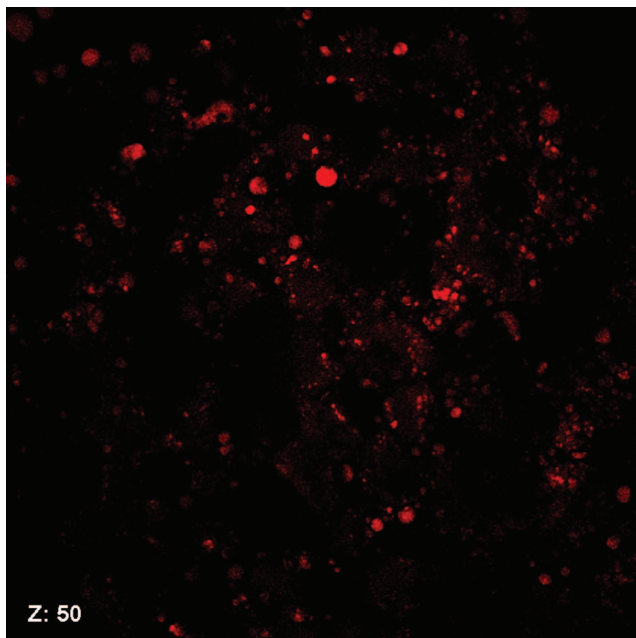

Fig. 4 (a) Changes in the contents of hepatic lipid droplets (the square root of CARS intensity), collagen fibrils (SHG intensity), and TPEF intensity in a BDL rat liver tissue with different time durations after BDL. (b) Correlation of SHG intensities with conventional histopathological scores of liver fibrosis. The fitted curve (dashed line) confirms the highly linear relationship ($I_{SHG} = 0.84 I_{score} - 1.16$; correlation factor $R^2 = 0.99$) of SHG versus histopathology scoring. Note that the error bars indicate the standard deviations (SD) of CARS, SHG, TPEF signals, and histopathological scores measured on the sectioned liver tissues; week 0 represents the control group, and weeks 1 to 6 denote the progression of liver disease at different time points after BDL surgery.

in the forward direction due to the phase-matching conditions. The epi-signals are usually very weak because of the destructive interference,[18] but the epi-CARS signals from the fine structures and interfaces can still be detectable due to the incomplete destructive interference.[18] The epi-CARS and SHG signals from thick tissue may still be detectable, as the generated forward nonlinear optical photons may encounter multiple scatterings in tissue, eventually redirecting CARS/SHG signals back into the epi-direction. To prove the above, an epi-detected 3D CARS scanning of a 2-mm thick liver tissue was performed. Video 3 shows the depth-resolved resonant CARS images acquired from the surface down to 70-μm depth of the liver tissue. The large lipid droplets (of up to 10 μm in size) have strong epi-CARS intensities due to the multiple scatterings of forward-propagating CARS photons. Another observation is that the CARS intensity first increases with the increasing scanning depth; then decreases gradually with tissue depth, but disappears after 66-μm depth. This probing depth is much shallower than that in the mouse ear's skin (125 μm)[19] probably due to a one-fold higher absorption coefficient in liver tissue as compared to skin tissues.[20] The major absorption in liver tissues arises from hemoglobin because of the widely distributed liver vasculature systems. SHG signals can also be detected in the epi-direction within a similar depth range in liver tissue (data not shown). However, due to the nonuniform biochemical distributions in biomedical tissue, Monte Carlo simulations on propagation of CARS/SHG photons in liver tissue should be conducted to more accurately evaluate how deep the nonlinear optical signals can be probed in tissue in the epi-detection mode.[21] Of course, to further move the integrated CARS and multiphoton microscopy imaging for non-invasive or minimally invasive liver tissue diagnosis and characterization, the development of a fiber-based ultrafast pulse laser system together with a rapid light scanning mechanism and miniaturized fiber probe design for effective excitation light delivery and tissue CARS/SHG/TPEF signals collection at laparoscopy is highly desirable.[22–25]

In summary, we have applied a multimodal nonlinear optical microscopy imaging technique developed to directly assess the progression of liver steatosis and fibrosis in a BDL rat liver model. The results show that the integrated CARS and multiphoton imaging technique provides new insights into distinct biochemical/biomolecular structures and compositions of tissue associated with liver steatosis and fibrosis transformation and thus has the potential to provide an effective means for early diagnosis and detection of liver disease without labeling.

References

1. E. Bjornsson and P. Angulo, "Non-alcoholic fatty liver disease," *Scand. J. Gastroenterol.* **42**(9), 1023–1030 (2007).
2. P. Angulo, "Nonalcoholic fatty liver disease," *N. Engl. J. Med.* **346**(16), 1221–1231 (2002).
3. R. Bataller and D. A. Brenner, "Liver fibrosis," *J. Clin. Invest.* **115**(2), 209–218 (2005).
4. A. Wieckowska, A. J. McCullough, and A. E. Feldstein, "Noninvasive diagnosis and monitoring of nonalcoholic steatohepatitis: present and future," *Hepatology* **46**(2), 582–589 (2007).
5. B. R. Masters and P. T. C. So, *Handbook of Biomedical Nonlinear Optical Microscopy*, Oxford University Press, Oxford (2008).
6. F. Lu, W. Zheng, C. Sheppard, and Z. Huang, "Interferometric polarization coherent anti-Stokes Raman scattering (IP-CARS) microscopy," *Opt. Lett.* **33**(6), 602–604 (2008).
7. F. Lu, W. Zheng, J. Lin, and Z. Huang, "Integrated coherent anti-Stokes Raman scattering and multiphoton microscopy for biomolecular imaging using spectral filtering of a femtosecond laser," *Appl. Phys. Lett.* **96**(13), 133701 (2010).
8. Y. Wu, H. Chen, W. Chang, J. Jhan, H. Lin, and I. Liau, "Quantitative assessment of hepatic fat of intact liver tissues with coherent anti-Stokes Raman scattering microscopy," *Anal. Chem.* **81**(4), 1496–1504 (2009).
9. E. Brown, T. McKee, E. di Tomaso, A. Pluen, B. Seed, Y. Boucher, and R. K. Jain, "Dynamic imaging of collagen and its modulation in tumors in vivo using second-harmonic generation," *Nat. Med.* **9**(6), 796–800 (2003).
10. D. C. S. Tai, N. Tan, S. Xu, C. H. Kang, S. M. Chia, C. L. Cheng, A. Wee, C. L. Wei, A. M. Raja, G. Xiao, S. Chang, J. C. Rajapakse, P. T. C. So, H. Tang, C. S. Chen, and H. Yu, "Fibro-C-Index: comprehensive, morphology-based quantification of liver fibrosis using second harmonic generation and two-photon microscopy," *J. Biomed. Opt.* **14**(4), 044013 (2009).
11. W. R. Zipfel, R. M. Williams, R. Christie, A. Y. Nikitin, B. T. Hyman, and W. W. Webb, "Live tissue intrinsic emission microscopy using multiphoton-excited native fluorescence and second harmonic generation," *Proc. Natl. Acad. Sci. U.S.A.* **100**(12), 7075–7080 (2003).
12. S. R. De Vriese, J. L. Savelii, J. P. Poisson, M. Narce, I. Kerremans, R. Lefebvre, W. S. Dhooge, W. De Greyt, and A. B. Christophe, "Fat absorption and metabolism in bile duct ligated rats," *Ann. Nutr. Metab.* **45**(5), 209–216 (2001).

13. S. F. Assimakopoulos and C. E. Vagianos, "Bile duct ligation in rats: A reliable model of hepatorenal syndrome?" *World J. Gastroenterol.* **15**(1), 121–123 (2009).

14. M. J. Ruwart, K. F. Wilkinson, B. D. Rush, T. J. Vidmar, K. M. Peters, K. S. Henley, H. D. Appelman, K. Y. Kim, D. Schuppan, and E. G. Hahn, "The integrated value of serum procollagen-III peptide over time predicts hepatic hydroxyproline content and staniable collagen in a model of dietart cirrhosis in the rat," *J. Hepatol.* **10**(5), 801–806 (1989).

15. G. Boigk, L. Stroedter, H. Herbst, J. Waldschmidt, E. O. Riecken, and D. Schuppan, "Silymarin retards collagen accumulation in early and advanced biliary fibrosis secondary to complete bile duct obliteration in rats," *J. Hepatol.* **26**(3), 643–649 (1997).

16. C. Xu and W. W. Webb, "Measurement of two-photon excitation cross sections of molecular fluorophores with data from 690 to 1050 nm," *J. Opt. Soc. Am. B* **13**(3), 481–491 (1996).

17. M. Zimmerley, C. Y. Lin, D. C. Oertel, J. M. Marsh, J. L. Ward, and E. O. Potma, "Quantitative detection of chemical compounds in human hair with coherent anti-Stokes Raman scattering microscopy," *J. Biomed. Opt.* **14**(4), 044019 (2009).

18. J. X. Cheng, A. Volkmer, and X. S. Xie, "Theoretical and experimental characterization of coherent anti-Stokes Raman scattering microscopy," *J. Opt. Soc. Am. B* **19**(6), 1363–1375 (2002).

19. C. L. Evans, E. O. Potma, M. Puoris'haag, D. Coˆté, C. P. Lin, and X. S. Xie, "Chemical imaging of tissue in vivo with video-rate coherent anti-Stokes Raman scattering microscopy," *Proc. Natl. Acad. Sci. U.S.A.* **102**(46), 16807–16812 (2005).

20. W. Cheong, S. A. Prahl, and A. J. Welch, "A review of the optical properties of biological tissues," *IEEE J. Quantum Elect.* **26**(12), 2166–2185 (1990).

21. J. Mo, W. Zheng, and Z. Huang, "Fiber-optic Raman probe couples ball lens for depth-selected Raman measurements of epithelial tissue," *Biomed. Opt. Express* **1**(1), 17–30 (2010).

22. A. Chong, J. Buckley, W. Renninger, and F. Wise, "All-normal-dispersion femtosecond fiber laser," *Opt. Express* **14**(21), 10095–10100 (2006).

23. Z. Huang, S. Teh, W. Zheng, J. Mo, K. Lin, X. Shao, K. Ho, M. Teh, and K. Yeoh, "Integrated Raman spectroscopy and tri-modal wide-field imaging techniques for real-time in vivo tissue Raman measurements at endoscopy," *Opt. Lett.* **34**(6), 758–760 (2009).

24. L. Fu and M. Gu, "Fibre-optic nonlinear optical microscopy and endoscopy," *J. Microsc.* **226**(3), 195–206 (2007).

25. A. Cuschieri, "Minimal access surgery and the future of interventional laparoscopy," *Am. J. Surg.* **161**(3), 404–407 (1991).